Role of Ocean Advections during the Evolution of the Pacific Meridional Modes

QI SHU,[a,b] YU ZHANG,[a,b] DILLON J. AMAYA,[c] SARAH M. LARSON,[d] YU KOSAKA,[e] JUN-CHAO YANG,[a,b] AND XIAOPEI LIN[a,b]

[a] *Physical Oceanography Laboratory, Frontier Science Center for Deep Ocean Multispheres and Earth System, Sanya Oceanographic Institution, Ocean University of China, Qingdao, Shandong, China*
[b] *Laoshan Laboratory, Qingdao, Shandong, China*
[c] *NOAA/Earth System Research Laboratory, Physical Science Laboratory, Boulder, Colorado*
[d] *Department of Marine, Earth, and Atmospheric Sciences, North Carolina State University, Raleigh, North Carolina*
[e] *Research Center for Advanced Science and Technology, The University of Tokyo, Tokyo, Japan*

(Manuscript received 24 April 2022, in final form 16 January 2023, accepted 3 March 2023)

ABSTRACT: The Pacific meridional modes (PMMs) are the leading ocean–atmosphere coupled modes in the subtropical northeastern (NPMM) and southeastern (SPMM) Pacific, respectively, and have been suggested to be key precursors to equatorial Pacific variability. Previous studies pointed out that both NPMM- and SPMM-related sea surface temperature (SST) anomalies are primarily driven by net surface heat flux variations during their equatorward evolution. However, whether oceanic heat advective processes would play a role during the evolution remains unclear. To address this issue, we perform an ocean mixed layer heat budget analysis based on observations and three ocean reanalysis datasets, and then reveal the effect of ocean advections on the evolution by comparing a fully coupled dynamic ocean model (DOM) to a slab ocean model (SOM). Our results suggest that for the NPMM evolution, ocean advections—primarily by anomalous meridional Ekman heat advections driven by mean and anomalous zonal wind stresses—play a damping role in the south of the NPMM. Thus, the NPMM SST anomalies appear to instead exhibit a poleward shift, although still freely propagating westward from the preceding boreal winter to the following summer. This finding challenges the traditional view that the NPMM propagates equatorward through the wind–evaporation–SST feedback. For the SPMM evolution, ocean advections play a damping role in the center of the SPMM from boreal spring to summer, as well as an intensification role in the southwest Pacific during summer. However, the effect of the intensification on the SPMM evolution is hard to determine due to the strong simulation bias of the SPMM evolution in the DOM.

SIGNIFICANCE STATEMENT: While it is known that both NPMM- and SPMM-associated SST anomalies are primarily driven by net surface heat flux variations during their evolution, whether ocean advections would play a role remains unknown. Here, we show that ocean advections play a role in the evolution of both PMMs. In particular, for the NPMM evolution, ocean advections play a damping role in the south of the NPMM center, causing a tendency for the NPMM to be displaced northward. The role of ocean advection challenges the prevailing notion that the NPMM simply evolves equatorward through the wind–evaporation–SST feedback.

KEYWORDS: Pacific Ocean; Ocean dynamics; Atmosphere–ocean interaction; Sea surface temperature; Anomalies; Climate variability

1. Introduction

The Pacific meridional modes (PMMs) are ocean–atmosphere coupled modes that occur in both the Northern and Southern Hemispheres and are characterized by distinct westward and equatorward sea surface temperature (SST) anomaly patterns extending from the subtropical eastern Pacific to the equatorial Pacific (Chiang and Vimont 2004; Amaya 2019). In the subtropical northeastern Pacific, it is called the North PMM (NPMM; Chiang and Vimont 2004); in the subtropical southeastern Pacific, it is termed the South PMM (SPMM; Zhang et al. 2014). By definition, both the NPMM and SPMM can occur independent of El Niño–Southern Oscillation (ENSO; Chiang and Vimont 2004; Min et al. 2017; You and Furtado 2018; Larson et al. 2018a; Zhang et al. 2021, 2022b) but have great impacts on the following ENSO occurrence (Chang et al. 2007; Larson and Kirtman 2013, 2014), ENSO spatial pattern (eastern Pacific vs central Pacific ENSO; Min et al. 2017; Stuecker 2018; Amaya 2019; Amaya et al. 2019; Chakravorty et al. 2021), and ENSO transitional processes (Kim and Yu 2021; Yeh et al. 2021).

The evolution of both PMMs can be divided into two stages: 1) the local development of the PMMs in the subtropical eastern Pacific, and 2) the propagation of the PMMs equatorward to the equatorial Pacific. During their development, both PMMs are primarily initiated by North and South Pacific atmospheric forcing, respectively. Specifically, the NPMM is primarily driven by the North Pacific Oscillation (NPO; Chiang and Vimont 2004; Amaya 2019; Zhang et al. 2021), a meridional dipole pattern of sea level pressure variability over the North Pacific, with one center of action over the

Supplemental information related to this paper is available at the Journals Online website: https://doi.org/10.1175/JCLI-D-22-0296.s1.

Corresponding author: Yu Zhang, zhangyu@ouc.edu.cn

DOI: 10.1175/JCLI-D-22-0296.1

Bering Strait and the other over the Hawaiian Islands (Walker and Bliss 1932; Rogers 1981; Zhang et al. 2022b). Similar to the NPMM, the SPMM is mainly forced by the South Pacific Oscillation (You and Furtado 2018; Zhang et al. 2021), a mirror of the NPO over the South Pacific (You and Furtado 2017). Apart from the North and South Pacific atmospheric forcing, both PMMs are also forced secondarily by shortwave radiation (Vimont et al. 2009; Alexander et al. 2010) while damped by ocean dynamical processes (You and Furtado 2018; Middlemas et al. 2019).

After the PMMs are initiated, they propagate equatorward to the equatorial Pacific through the wind–evaporation–SST (WES; Xie and Philander 1994) feedback (Chiang and Vimont 2004; Vimont et al. 2009; Wu et al. 2010; Zhang et al. 2014; Ma et al. 2017; Min et al. 2017; Larson et al. 2018a; You and Furtado 2018; Amaya 2019; Amaya et al. 2019; Yang et al. 2022). The positive phase of the NPMM (warm SST anomalies), for example, induces surface southwesterly anomalies on its southwest flank, which converge toward the center of the warmest SST anomalies associated with the NPMM. The southwesterly anomalies further relax the northeasterly trade winds, driving underlying, downward, latent heat fluxes and further reinforcing the positive SST anomalies. This WES feedback, as a result, gives rise to the NPMM propagating southwestward to the equator. Similar to the NPMM propagation process, the SPMM propagates northwestward to the equator through the WES feedback (Zhang et al. 2014; Min et al. 2017; Larson et al. 2018a; You and Furtado 2018).

While the WES feedback-induced evolution of the PMMs has been extensively investigated, the role of ocean dynamics during the PMMs' evolution remains unclear. Ocean dynamics, however, have been invoked to describe the amplification of SPMM-related SST anomalies in the eastern equatorial Pacific after the SPMM has reached the equator (Larson et al. 2018a). Additionally, ocean dynamics have also been invoked to explain the ocean response to the NPO. According to the so-called trade wind charging mechanism, the anomalous wind stress curl associated with the NPO drives an equatorward ocean transport that primes the equatorial Pacific for an ENSO event. (Anderson 2007; Anderson et al. 2013; Anderson and Perez 2015). There is a reason to believe that wind variability could also drive ocean dynamical effects near the ocean surface that would influence the SST anomalies associated with the PMMs. For example, anomalous wind stress–driven Ekman a dvection generally damps SST anomalies driven by turbulent heat flux anomalies in the large-scale subtropical oceans (Larson et al. 2018b; Small et al. 2020). In particular, Takahashi et al. (2021) demonstrated that this Ekman damping effect, indeed, modifies SST variability in the subtropical Pacific near Hawaii. Therefore, we are motivated to investigate the potential role of ocean advective processes during the PMMs' surface evolution. It should be noted that ocean advections do not necessarily play roles in the region of PMM development and along the path of equatorward propagation; they could play roles in the vicinity of the PMMs, affecting the behavior of PMMs' evolution.

To investigate this issue, we first diagnose the role of ocean advections during the PMMs' evolution based on a mixed layer heat budget analysis in three ocean reanalysis products. Then, to reveal the effect of the ocean advections, we compare the PMMs' evolution in a fully coupled dynamic ocean model (DOM) to that in a slab ocean model (SOM). Our results show that for the NPMM evolution, ocean advections play a damping role in the south of the NPMM center resulting in the NPMM shifting northward and freely propagating westward. For the SPMM, ocean advections play a damping role in the SPMM center and an intensification role in the southwest Pacific; the effect of the latter role is unclear due to the large uncertainty across the three reanalysis datasets and the simulation bias in the DOM. Our finding on the role of ocean advections during the NPMM evolution challenges the traditional view that the NPMM propagates equatorward through the thermodynamically coupled WES feedback.

The remainder of the paper is organized as follows. Section 2 introduces observational and reanalysis datasets, the configurations of the SOM and DOM, the mixed layer heat budget analysis, as well as preliminary data processing methods. Section 3 and section 4 investigate the role of ocean advections during the NPMM evolution and the SPMM evolution, respectively. A summary with discussion is presented in section 5.

2. Data and methods

a. Observational and reanalysis data

To depict the spatiotemporal evolution of the PMMs, we use observational SSTs from the Hadley Centre Sea Ice and Sea Surface Temperature, version 1.1 (HadISSTv1.1), dataset (Rayner et al. 2003) with a horizontal resolution of 1° longitude × 1° latitude. In addition, we also use 10-m wind from the atmospheric reanalysis product of the NOAA–CIRES–DOE Twentieth Century Reanalysis, version 3 (20CRv3; Slivinski et al. 2019), with a horizontal resolution of 1° longitude × 1° latitude. To diagnose the roles of ocean advections on the PMMs' evolution, we use three oceanic reanalysis datasets: 1) the second German contribution to Estimating the Circulation and Climate of the Ocean system (GECCO2) with a horizontal resolution of 1° longitude × 1° latitude and 50 vertical levels (Köhl 2015); 2) the Ocean Reanalysis System 3 (ORAS3) with a horizontal resolution of 1° longitude × 1° latitude and 29 vertical levels (Balmaseda et al. 2008); and 3) the Simple Ocean Data Assimilation, version 2.2.4 (SODA2.2.4), with a horizontal resolution of 0.5° longitude × 0.5° latitude and 40 vertical levels (Carton and Giese 2008). For the horizontal resolution of the SODA2.2.4, to be consistent with that of the other two oceanic reanalysis products, horizontal grids are linearly interpolated into 1° longitude × 1° latitude. For the GECCO2 and ORAS3, we use the variables of temperature, net heat flux, and 3D ocean currents; for the SODA2.2.4, we only use the variables of temperature and 3D ocean currents, since the outputs of heat flux data are not provided. All the above data used in this study are monthly means and are from 1959 to 2009, the largest overlapping period across all the observational and reanalysis datasets.

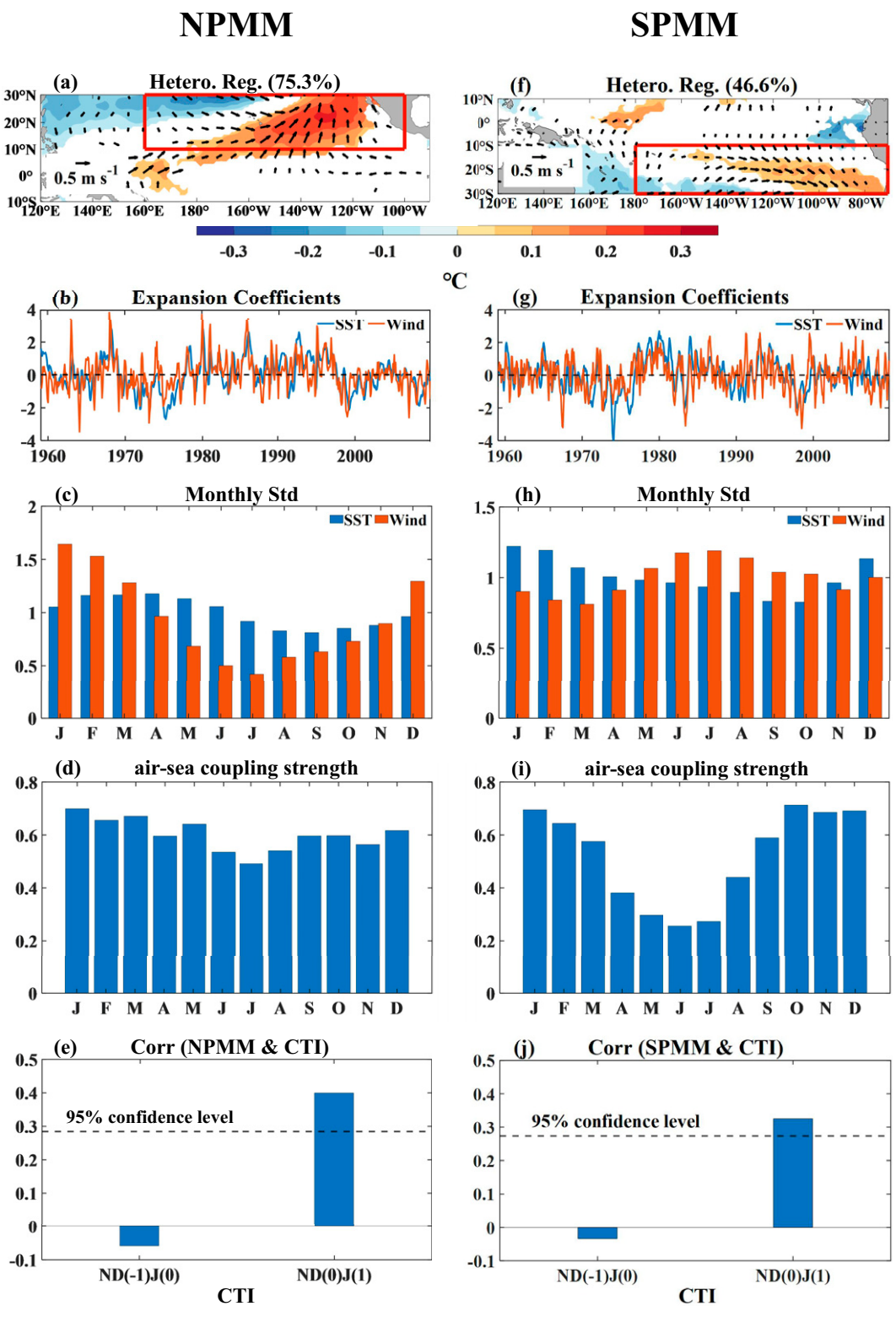

FIG. 1. Spatiotemporal characteristics of the observed (left) NPMM and (right) SPMM. (a),(f) Heterogenous regressions of SST (shading; °C) and 10-m wind (vectors; m s^{-1}) anomalies against SVD-derived, normalized expansion coefficients (see details in section 2c). Only the regressions significant at the 95% confidence level based on a two-tailed Student's *t* test are shown. Red boxes represent the corresponding SVD domain. Squared covariance fractions are marked in the parentheses of the titles. (b),(g) Normalized SST (blue) and 10-m wind (red) expansion coefficients. (c),(h) Climatological standard deviations of the normalized SST and 10-m wind expansion coefficients in each calendar month. (d),(i) Correlations of SST expansion coefficient with 10-m wind expansion coefficient in each calendar month. (e),(j) Correlations of the corresponding PMM index with preceding (left bar) and following (right bar) NDJ CTI.

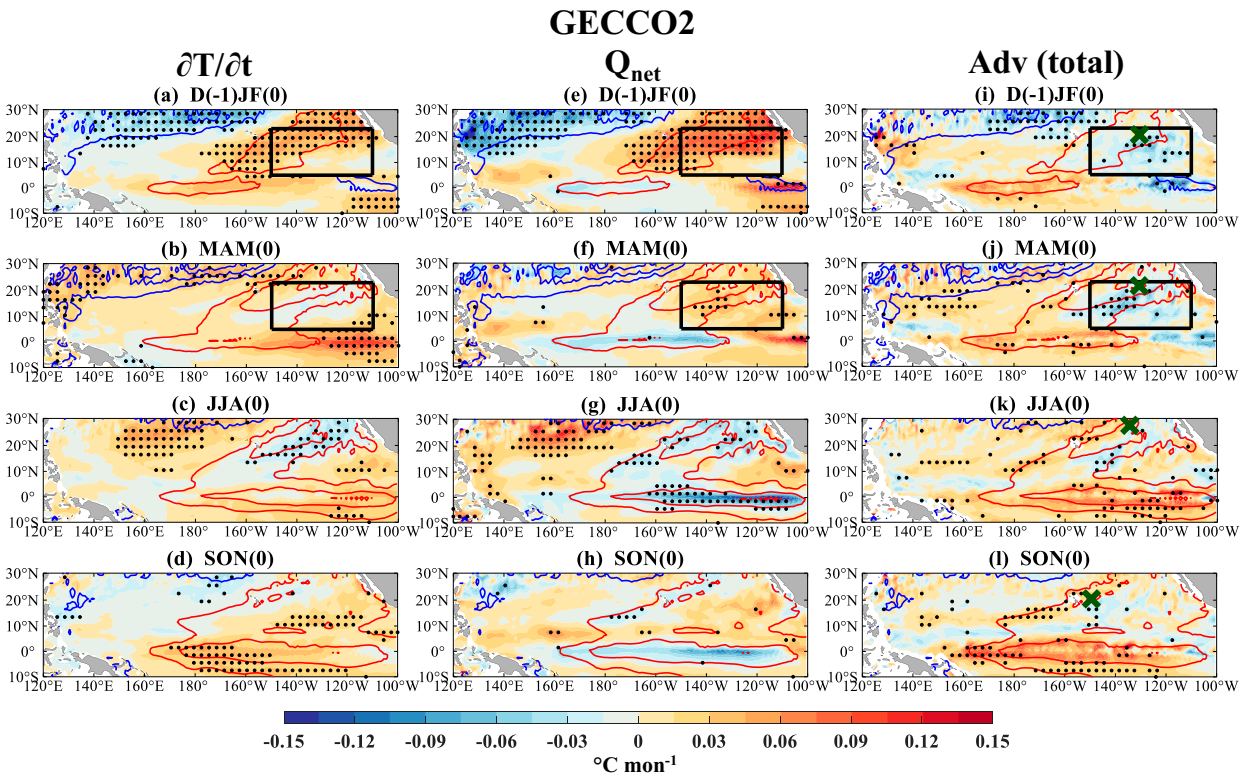

FIG. 2. Evolution of the NPMM-associated MLT and heat flux terms from D(−1)JF(0) to SON(0) in the GECCO2. Patterns are regressions of the tendency of (left) MLT anomalies (shading; °C month^{-1}), (center) net surface heat flux (shading; °C mon^{-1}), and (right) total oceanic heat advection anomalies (shading; °C mon^{-1}) against the NPMM index. The stippling indicates statistical significance at the 95% confidence level based on a two-tailed Student's *t* test. Contours in all the panels are the regressed MLT anomalies (red is positive, blue is negative; contour interval: 0.1°C). Black boxes and green markers represent the domain of 5°–23°N, 150°–110°W and the center of the NPMM (maximum value of the positive MLT anomalies in the subtropics), respectively.

b. SOM and DOM

To demonstrate the effects of ocean advections on the PMMs' evolution, we employ two model experiments, both based upon the Geophysical Fluid Dynamic Laboratory coupled model, version 2.1 (CM2.1; Delworth et al. 2006). The first is the SOM: the atmosphere coupled with a motionless slab ocean (i.e., in the absence of mean and anomalous ocean currents) with 50-m constant mixed layer depth (MLD) globally. By the design, ocean temperature in the mixed layer varies only through air–sea thermodynamic coupling processes. The second is the DOM: the atmosphere coupled with dynamic ocean (i.e., in the presence of mean and anomalous ocean currents) with spatiotemporally varied MLD. By this configuration, mixed layer temperature evolves through both air–sea thermodynamic and dynamic coupling processes. Therefore, comparing the PMMs' evolution in the SOM to that in the DOM demonstrates the effects of ocean dynamics (mean and anomalous ocean currents). The SOM simulation is 100 years and publicly available online (see data availability statement section). To be consistent with the simulation length of the SOM, we use the first 100-yr output from a 1000-yr DOM simulation employed in Zhang et al. (2022a). More details of the configurations of the two experiments can be referred to Zhang et al. (2022a).

c. Preliminary data processing

To isolate seasonal variations associated with the PMMs, we apply a 3-month running mean after the removal of the monthly climatology and linear trend. To characterize the spatiotemporal variability of the NPMM and SPMM, we perform a singular value decomposition (SVD) analysis between SST and 10-m wind anomalies after linear removing of the cold tongue index (CTI; 6°S–6°N, 180°–90°W; Deser and Wallace 1990) month by month (i.e., simultaneous removal, following the method of Zhang et al. 2021), in the subtropical northeastern (10°–30°N, 160°E–100°W) and southeastern Pacific (30°–10°S, 180°–70°W), respectively (red boxes in Figs. 1a,f).

Figure 1 shows the spatiotemporal variability of the NPMM and SPMM based on the HadISSTv1.1 and 20CRv3. We use the SVD analysis–derived 10-m wind rather than the SST expansion coefficient to represent NPMM and SPMM variability because 1) we are interested in ocean advections, which are typically forced by surface wind variability; 2) the 10-m

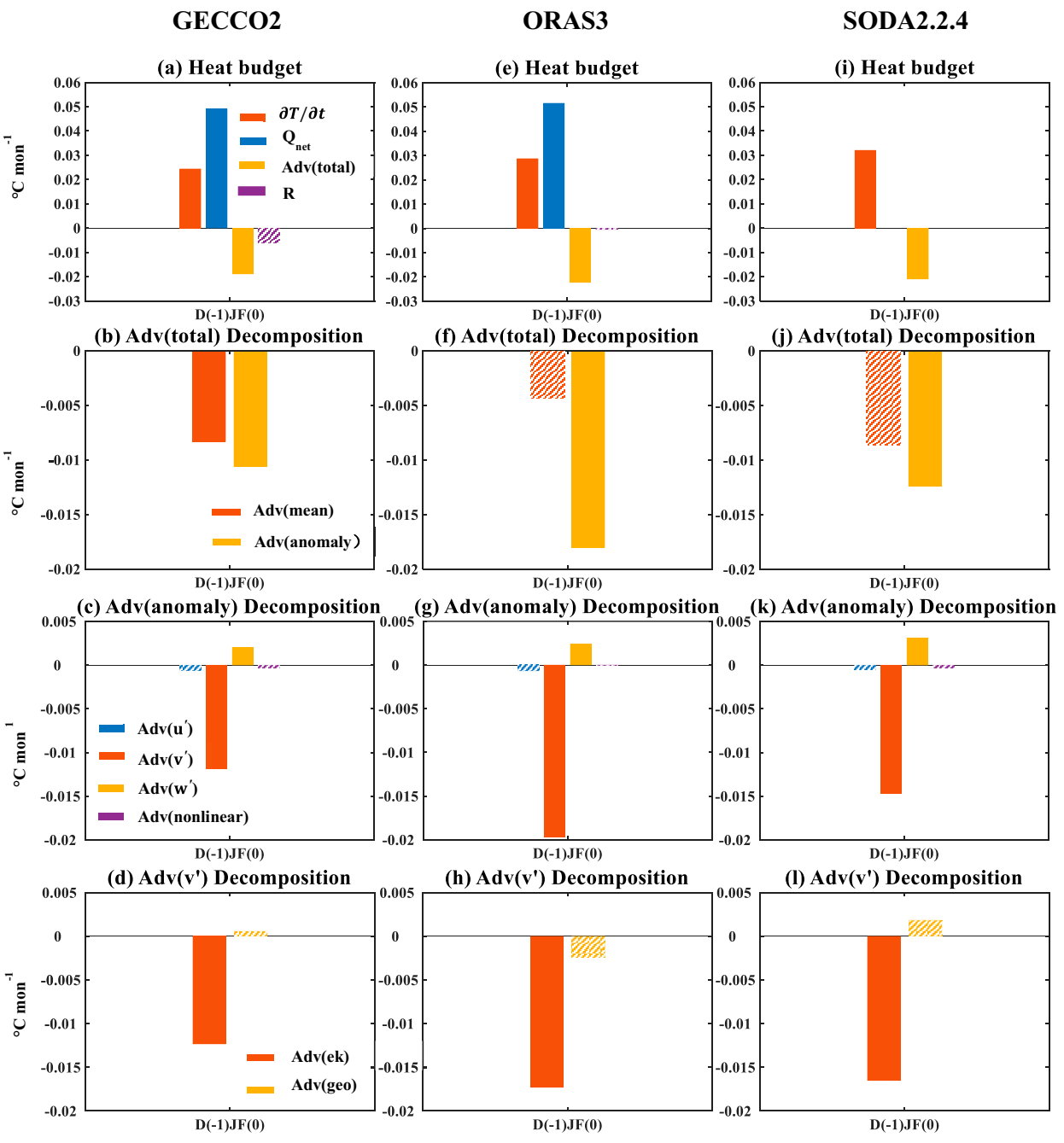

FIG. 3. Regressions of NPMM-associated heat budget terms in D(−1)JF(0) in the black box of Fig. 2 against the NPMM index in the (left) GECCO2, (center) ORAS3, and (right) SODA2.2.4. (a),(e),(i) Regressed tendency of MLT anomalies (red), net surface heat flux (blue), total heat advection (yellow), and residual term (purple). (b),(f),(j) Decomposition of total heat advection into the terms associated with the mean (red) and anomalous (yellow) ocean current, respectively. (c),(g),(k) Decomposition of the term associated with the anomalous ocean current. (d),(h),(l) Decomposition of the linear term associated with the anomalous meridional current into Ekman (red) and geostrophic (yellow) heat advections. Solid (slashed) bars are statistically significant (insignificant) at the 95% confidence level.

wind expansion coefficients for both PMMs are largely unaffected by the nonlinearity of the CTI (Min et al. 2017; You and Furtado 2018), compared to the SST expansion coefficients (Chiang and Vimont 2004); and 3) the 10-m wind expansion coefficients for both PMMs' evolution were used in recent studies (Min et al. 2017; You and Furtado 2018). Furthermore, we define the January–March (JFM) and February–April (FMA) averaged, normalized, 10-m wind expansion coefficient as NPMM and SPMM indices. We use these definitions because 1) for the NPMM, 10-m wind variability is

strongest in JFM (red bars in Fig. 1c), and air–sea coupling strength, defined as correlations between 10-m wind and SST expansion coefficient month by month (You and Furtado 2018), is also strongest during the three months (Fig. 1d); 2) for the SPMM, although 10-m wind variability is not strong in FMA (strongest in June–August; Fig. 1h), air–sea coupling strength during the three months is relatively strong (Fig. 1i); additionally, using the FMA 10-m wind expansion coefficient as the SPMM index was employed in the previous studies (Min et al. 2017; You and Furtado 2018); and 3) the JFM NPMM index and FMA SPMM index are largely independent of preceding winter ENSO events, illustrated by the insignificant correlations with previous November–January (NDJ) CTI (left bar in Figs. 1e,j); note that they significantly correlate with the following NDJ CTI (right bar in Figs. 1e,j), suggesting that both PMMs can evolve into ENSO-like events, as demonstrated by previous studies (e.g., Chiang and Vimont 2004; Zhang et al. 2014; Ma et al. 2017; Min et al. 2017; Larson et al. 2018a; You and Furtado 2018; Amaya 2019; Amaya et al. 2019; Yang et al. 2021).

d. A mixed layer heat budget analysis

To quantify the roles of ocean advections during the evolution of the NPMM and SPMM, we conduct a mixed layer heat budget analysis:

$$\frac{\partial T'}{\partial t} = \frac{Q'_{\text{net}}}{\rho c_p H} - \overline{u}\frac{\partial T'}{\partial x} - \overline{v}\frac{\partial T'}{\partial y} - \overline{w}\frac{T' - T'_d}{H} - u'\frac{\partial \overline{T}}{\partial x} - u'\frac{\partial T'}{\partial x} - v'\frac{\partial \overline{T}}{\partial y} - v'\frac{\partial T'}{\partial y} - w'\frac{\overline{T} - \overline{T}_d}{H} - w'\frac{T' - T'_d}{H} + R, \quad (1)$$

where the overbar denotes monthly climatology and prime denotes monthly anomaly; T is mixed layer temperature (MLT); Q_{net} is net surface heat flux (note that we do not introduce solar penetration here, because the shortwave radiation flux is unavailable in the ORAS3 and SODA2.2.4 reanalysis datasets; introducing it only to the GECCO2 will not compare the heat budget results to the ORAS3 and SODA2.2.4); ρ is the density of seawater of 1022.4 kg m^{-3}; c_p is the specific heat of seawater at constant pressure, which is 3940 J kg^{-1} °C^{-1}; H is monthly climatological MLD with seasonal cycle, defined as the depth at which potential temperature is smaller than 5-m potential temperature for 0.5°C (Kim et al. 2007); u and v are the zonal and meridional current velocities averaged over MLD, respectively; w is entrainment velocity, formulated as $\partial H/\partial t + u_d\partial H/\partial x + v_d\partial H/\partial y + w_d$ (u_d, v_d, and w_d are zonal, meridional, and vertical velocities, respectively, at the bottom of MLD), following Stevenson and Niiler (1983); T_d is potential temperature at the bottom of MLD; and R is a residual term, including processes such as mixing and the neglected solar penetration.

In Eq. (1), main physical processes governing the tendency of mixed layer temperature variation can be categorized into three groups: net surface heat flux forcing (the first term on the right-hand side [RHS]), heat advection by mean ocean current (the second to the fourth terms on the RHS), and heat advection by anomalous ocean current, which involves both linear and nonlinear dynamical heating processes (the fifth to the second-to-last terms on the RHS).

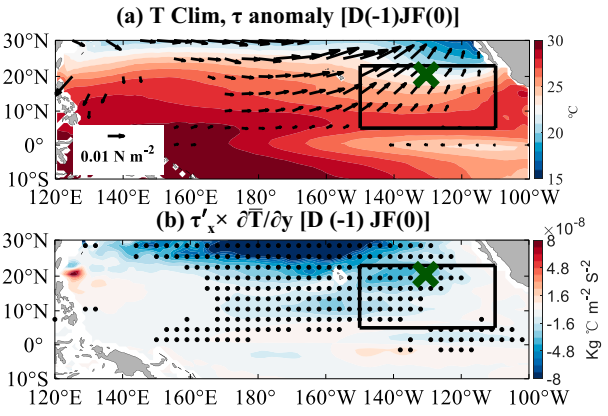

FIG. 4. (a) MLT climatology (shading; °C) in DJF and NPMM-associated wind stress anomalies (vectors; N m^{-2}) in D(−1)JF(0). (b) Regressions of NPMM-associated zonal wind stress anomalies in D(−1)JF(0) multiplied by the meridional gradient of DJF MLT climatology against the NPMM index. Stippling indicates statistical significance at the 95% confidence level. Black boxes and green markers are the same as those in the first two rows of Fig. 2.

To explore whether the effect of horizontal heat advection [the terms including u and v in Eq. (1)] during the PMMs' evolution is attributed to Ekman or geostrophic heat advection, we compute the Ekman heat advection [with the same unit as the heat budget terms of Eq. (1)] derived from the vector quantity wind stress ($\boldsymbol{\tau}$) and the scalar quantity T, which is given by$[(\mathbf{k}\times\boldsymbol{\tau})\cdot\nabla T]/f\rho H$, where f is the Coriolis parameter, and $\mathbf{k}$ is a unit normal vector. The geostrophic heat advection is obtained simply by subtracting the Ekman heat advection from the horizontal heat advection. It is worth noting that we only calculate the Ekman and geostrophic heat advections outside the equatorial Pacific (5°S–5°N), since the above computing methods are not suitable for the region in which f is small.

3. Role of ocean advections during the evolution of the NPMM

a. Diagnoses from the observational and reanalysis datasets

We first diagnose the role of ocean advections during the evolution of the NPMM based on the heat budget analysis. To do so, we regress the tendency of MLT anomalies, net surface heat flux, and total oceanic heat advection anomalies [the summation of the second to the second-to-last terms on the RHS of Eq. (1)] against the NPMM index from boreal winter {December–February [D(−1)JF(0)]} to the following fall {September–November [SON(0)]} in the GECCO2 and ORAS3, respectively (shading in Fig. 2 and Fig. S1 in the online supplemental material). In addition, we also regress the anomalies, except net surface heat flux, against the NPMM index in the SODA2.2.4 (Fig. S2). We will not show the regressed patterns in the following D(0)JF(1), as the PMMs are

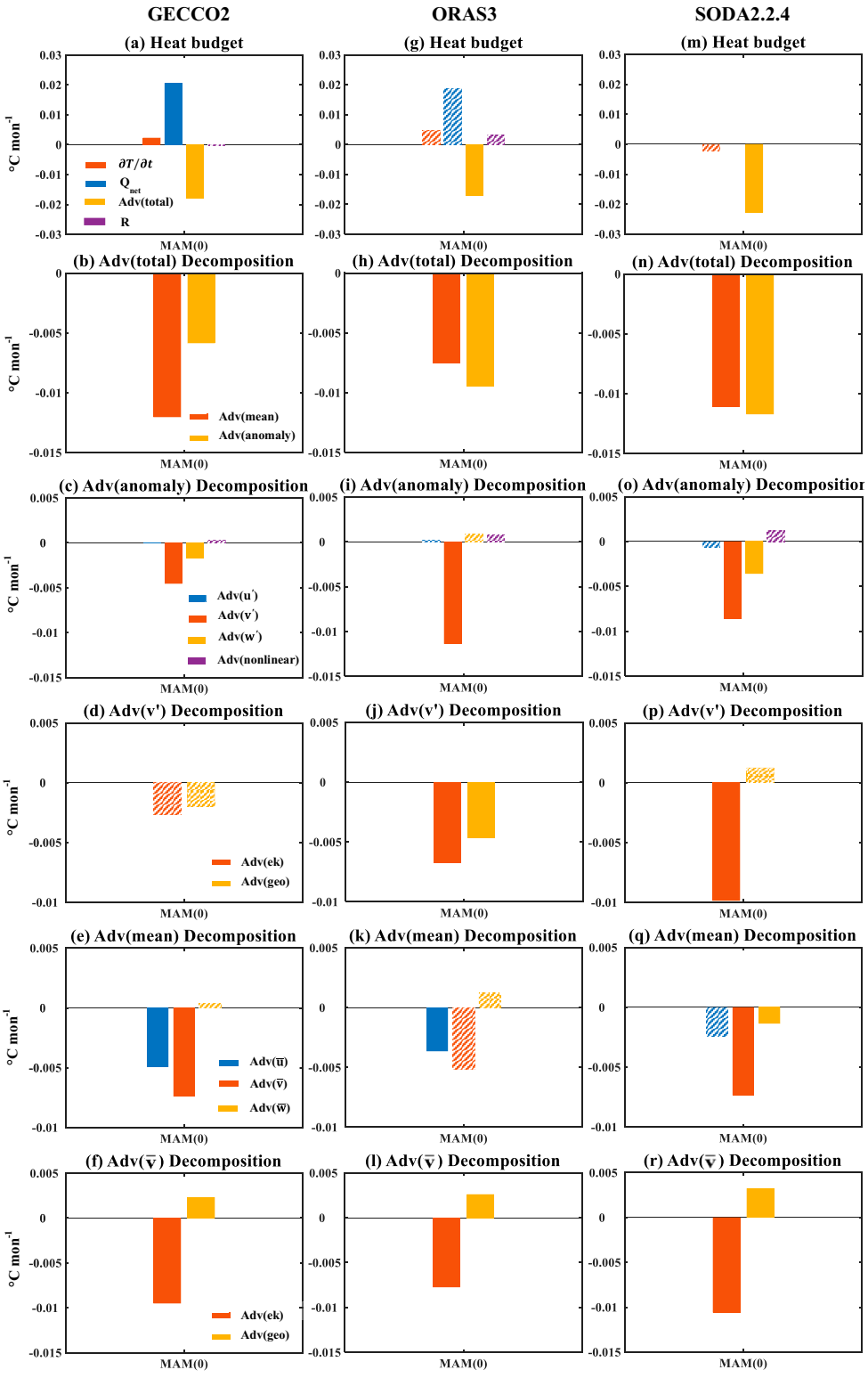

FIG. 5. As in Fig. 3, but for MAM(0).

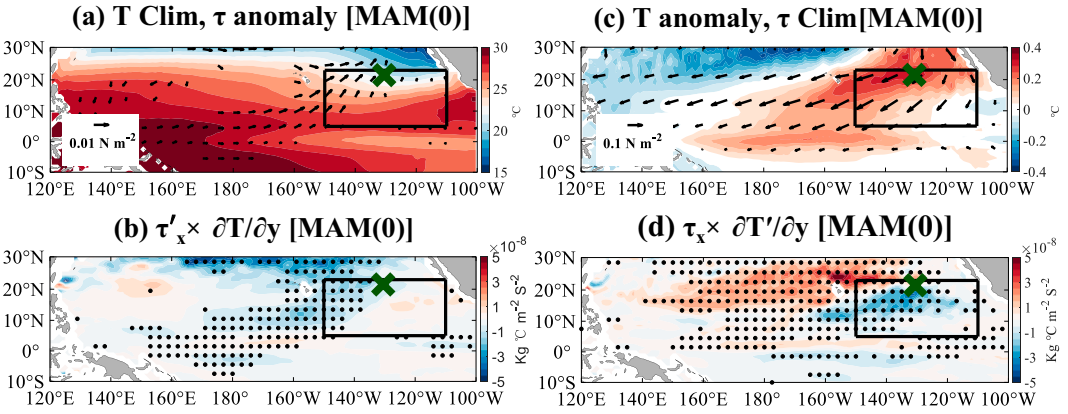

FIG. 6. (a),(b) As in Fig. 4, but for MAM(0). (c) NPMM-associated MLT anomalies (shading; °C) in MAM(0) and wind stress climatology (vectors; N m^{-2}) in MAM. (d) Regressions of zonal wind stress climatology in MAM multiplied by meridional gradient of NPMM-associated MAM(0) MLT anomalies against the NPMM index.

generally faded out during the season (e.g., Vimont et al. 2009). In this study, numbers 0, −1, and 1 represent contemporaneous year, previous year, and following year of PMM variability, respectively. The regressions statistically significant at the 95% confidence level based on a two-tailed Student's t test are dotted. In addition to these regressed variables, MLT anomalies are also regressed (contours in Fig. 2, Figs. S1 and S2) against the NPMM index (the region including NPMM evolution to ENSO events in the equatorial Pacific).

The results show that, overall, the NPMM evolution is governed by net heat flux anomalies north of the equator (cf. left and center columns of Fig. 2 and Fig. S1), consistent with previous studies (Chiang and Vimont 2004; Ma et al. 2017; Min et al. 2017; Amaya 2019; Amaya et al. 2019). However, the NPMM evolution is also affected by oceanic heat advections (right columns of Fig. 2, Figs. S1 and S2). Specifically, in D(−1)JF(0), oceanic heat advections act to damp MLT anomalies south of the center of the NPMM, albeit the weakest in the SODA2.2.4 (black boxes and green markers in

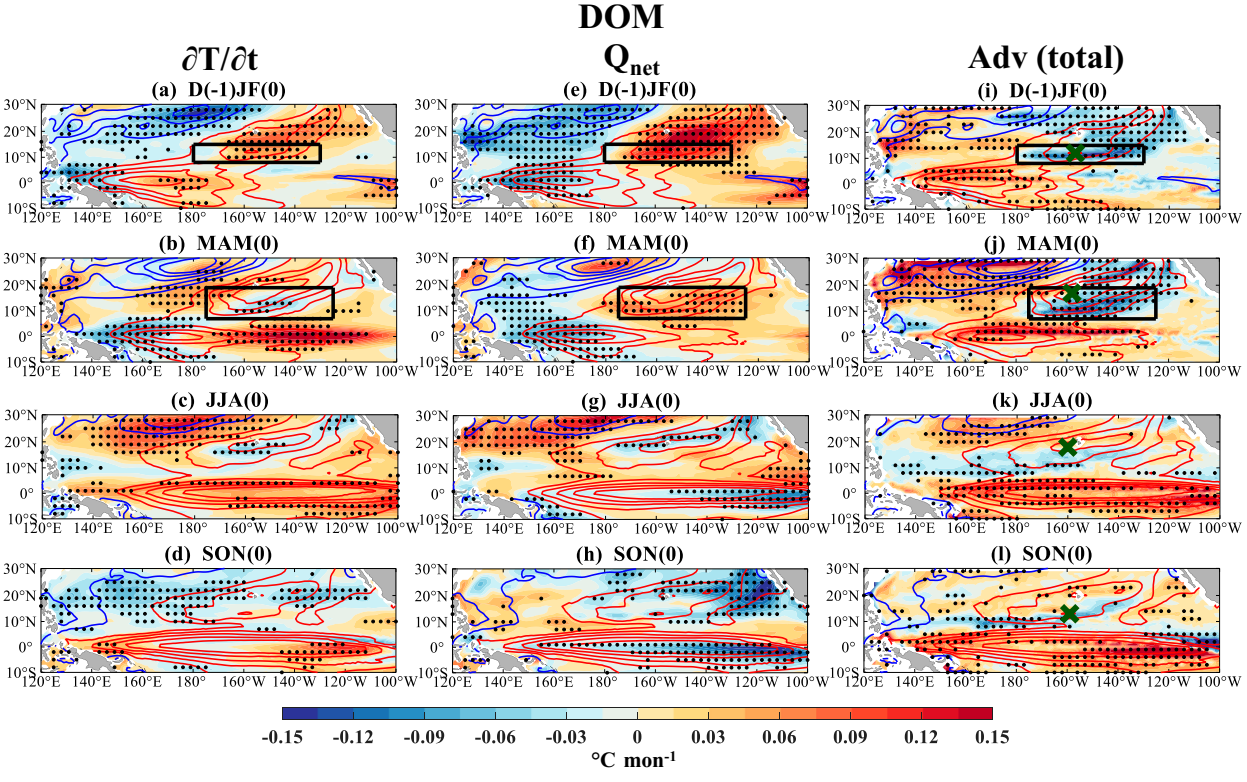

FIG. 7. As in Fig. 2, but for the NPMM evolution in the DOM.

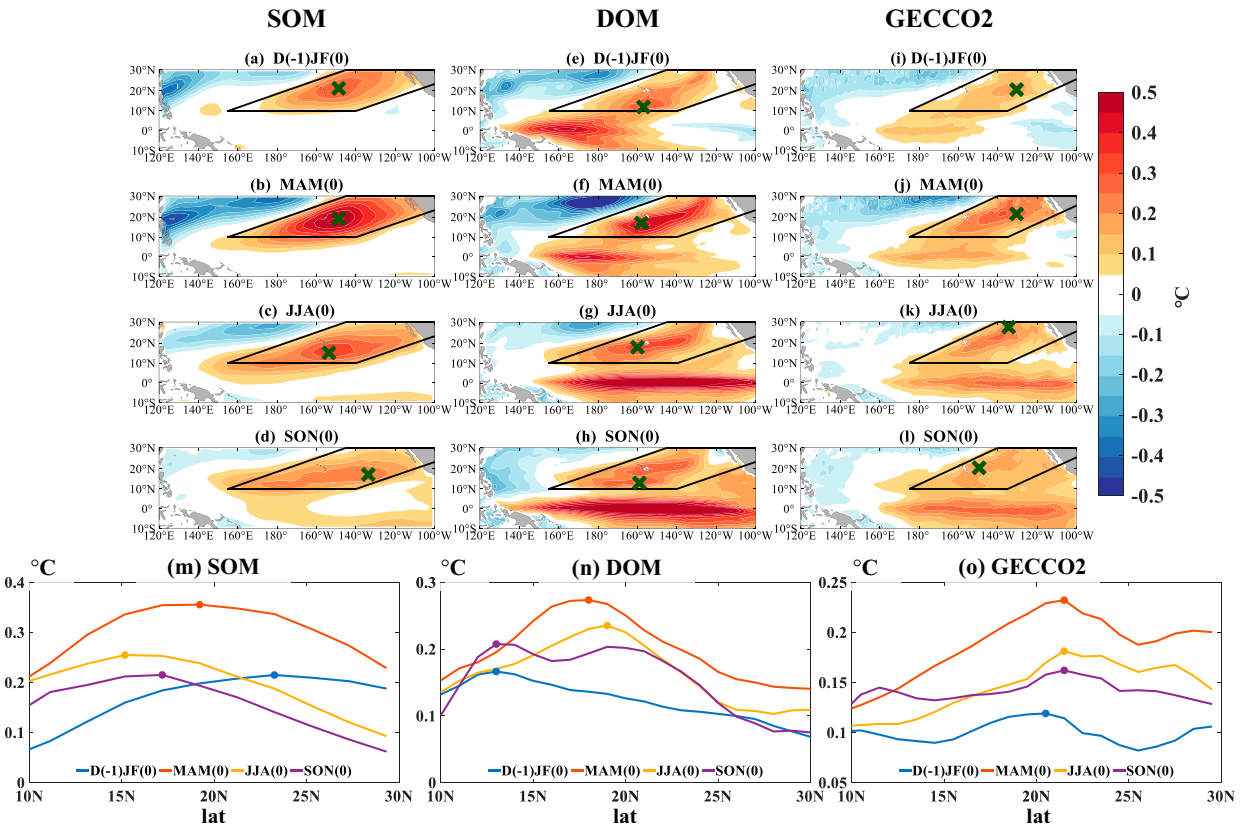

FIG. 8. Comparison of the evolution of NPMM-associated MLT anomalies between the (a)–(d) SOM and (e)–(h) DOM. (i)–(l) NPMM-associated MLT anomalies in the GECCO2. Green markers represent the center of the NPMM-associated MLT anomalies. (m)–(o) Zonally averaged NPMM-associated MLT anomalies in the region enclosed by the black lines in the SOM, DOM, and GECCO2, respectively.

Fig. 2i, Figs. S1i and S2e). They compensate 38% (43% in the ORAS3) of the intensification effect by net heat flux anomaly (black boxes in Fig. 2e and Fig. S1e), calculated by absolute value of the yellow bar in Fig. 3a (Fig. 3e) divided by the blue bar in Fig. 3a (Fig. 3e). As a result, the tendency of NPMM-related MLT anomalies therein is moderately positive (black boxes in Fig. 2a and Fig. S1a).

To reveal which ocean advective processes primarily contribute to this damping effect, we regress the anomalous heat advections by mean and anomalous ocean current averaged over that domain in D(−1)JF(0) against the NPMM index, respectively (the second row of Fig. 3). The results show that anomalous heat advection by the anomalous ocean current significantly dominates the damping effect. Further decomposition of the anomalous heat advection indicates that the damping effect is attributed to the linear heat budget term associated with the anomalous meridional current (the third row of Fig. 3). This term is further decomposed into Ekman and geostrophic heat advection; the result shows that the former plays a key role (the last row of Fig. 3).

To understand why the anomalous, zonal, wind-driven meridional Ekman heat advection dominates the damping effect, we regress D(−1)JF(0) wind stress anomalies against the NPMM index and superimpose DJF MLT climatology, illustrated by the GECCO2 (Fig. 4a). It is found that the MLT climatology exhibits strong meridional gradient south of the center of the NPMM. As a result, the westerly component of the NPMM-related wind stress anomalies induces southward Ekman heat advection, which cools the relatively warm climatological MLT in the south [negative values in the black box of Fig. 4b, computed by multiplying the NPMM-related D(−1)JF(0) zonal wind stress anomalies by the meridional gradient of DJF MLT climatology].

In the following MAM(0), the oceanic damping effect south of the center of the NPMM sustains (Fig. 2j, Figs. S1j and S2f). The heat budget analysis suggests that the damping effect almost compensates the intensification effect by the net heat flux anomaly, resulting in the weak MLT tendency (first row of Fig. 5). Further decomposition shows that the damping effect is contributed by the anomalous heat advection not only from the anomalous ocean current but also from the mean ocean current (second row of Fig. 5). The magnitudes of both components are comparable in the ORAS4 and SODA2.2.4 but are twice that for the mean ocean current in the GECCO2. Further decomposition of the heat advection by the anomalous ocean current indicates that anomalous meridional Ekman heat advection plays the dominant role, albeit a less significant one in the GECCO2 (third and fourth rows

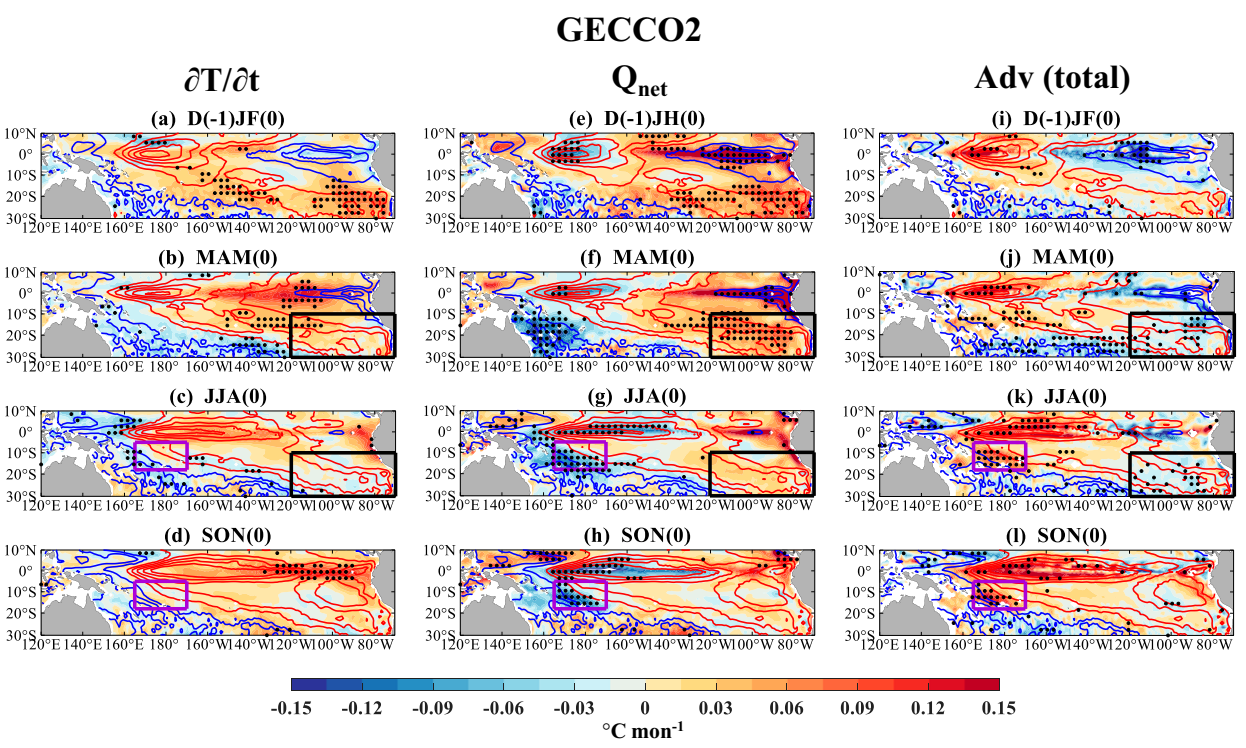

FIG. 9. As in Fig. 2, but for the evolution of the SPMM in the GECCO2 from D(−1)JF(0) to SON(0). Black boxes in the second and third rows represent the domain of 30°–10°S, 120°–70°W. Purple boxes in the last two rows represent the domain of 18°–5°S, 165°E–170°W.

of Fig. 5). For the contribution from the mean ocean current, heat budget decomposition shows that the mean meridional Ekman heat advection is dominant (last two rows of Fig. 5).

To understand why both anomalous and mean meridional Ekman heat advections contribute to the oceanic damping effect in MAM(0), we plot the related maps of climatological and regressed wind stress and MLT against the NPMM index in the GECCO2 (Fig. 6). It is found that during boreal spring, although the NPMM-related wind stress anomalies are weaker than those in the preceding winter (cf. Figs. 4a and 6a), the meridional mean MLT gradient remains strong, resulting in the prominent, anomalous, westerly wind–driven, southward Ekman heat advection (Fig. 6b). Concurrently, the NPMM-related MLT anomalies are strongest (Fig. 2). As a result, climatological easterly trade winds (Fig. 6c) induce a strong northward Ekman heat advection anomaly, damping the south of center of the NPMM (Fig. 6d).

b. *Model simulations*

Based on the heat budget analysis applied to the reanalysis datasets, we have shown that ocean advections play a damping role in the south of the center of the NPMM during boreal winter and spring. Yet, how the damping role affects the NPMM's evolution remains unclear. Thus, this section will demonstrate the effect by comparing the DOM to the SOM simulation.

Before the comparison, we need to assess the simulation skill of the spatiotemporal variability of the NPMM in the DOM (Fig. S3). The result shows that the simulation has some biases compared to the observations (left column of Fig. 1). First, the amplitude of the NPMM is too strong, and its center is located around the Hawaiian Islands (Fig. S3a) while it develops from the west coast of Baja California in the observations (Fig. 1a). Second, the NPMM-related 10-m wind variability exhibits two peaks—one in January–March, similar to the observations (Fig. 1c), and the other in August–October (Fig. S3c). Third, the air–sea coupling strength is strongest in late summer to early fall (Fig. S3d), while it is strongest in boreal winter in the observations (Fig. 1d). Despite of these biases, the DOM captures the essential spatiotemporal characteristics of the NPMM.

Moreover, we also need to evaluate the simulation skill of the evolution of the NPMM-related MLT and heat flux terms anomalies (Fig. 7). Overall, the DOM simulates the evolution well compared to the reanalysis datasets (Fig. 2, Figs. S1 and S2). Importantly, the DOM captures the oceanic damping effect during boreal winter and spring, albeit with significant signals north of the center of the NPMM (Figs. 7i,j). Nevertheless, the stronger oceanic damping roles around and south of the center of the NPMM (black boxes in Fig. 7) are consistent with the reanalysis products. Therefore, comparing the NPMM's evolution in the DOM to that in the SOM provides insight into revealing the roles of the oceanic damping effects.

Figure 8 shows the comparison of the evolutions of NPMM-related MLT anomalies between the SOM and DOM. In the SOM, the NPMM-related MLT anomalies originate from the east of the Hawaiian Islands during boreal winter (Fig. 8a). Subsequently, the anomalies become strongest in boreal spring

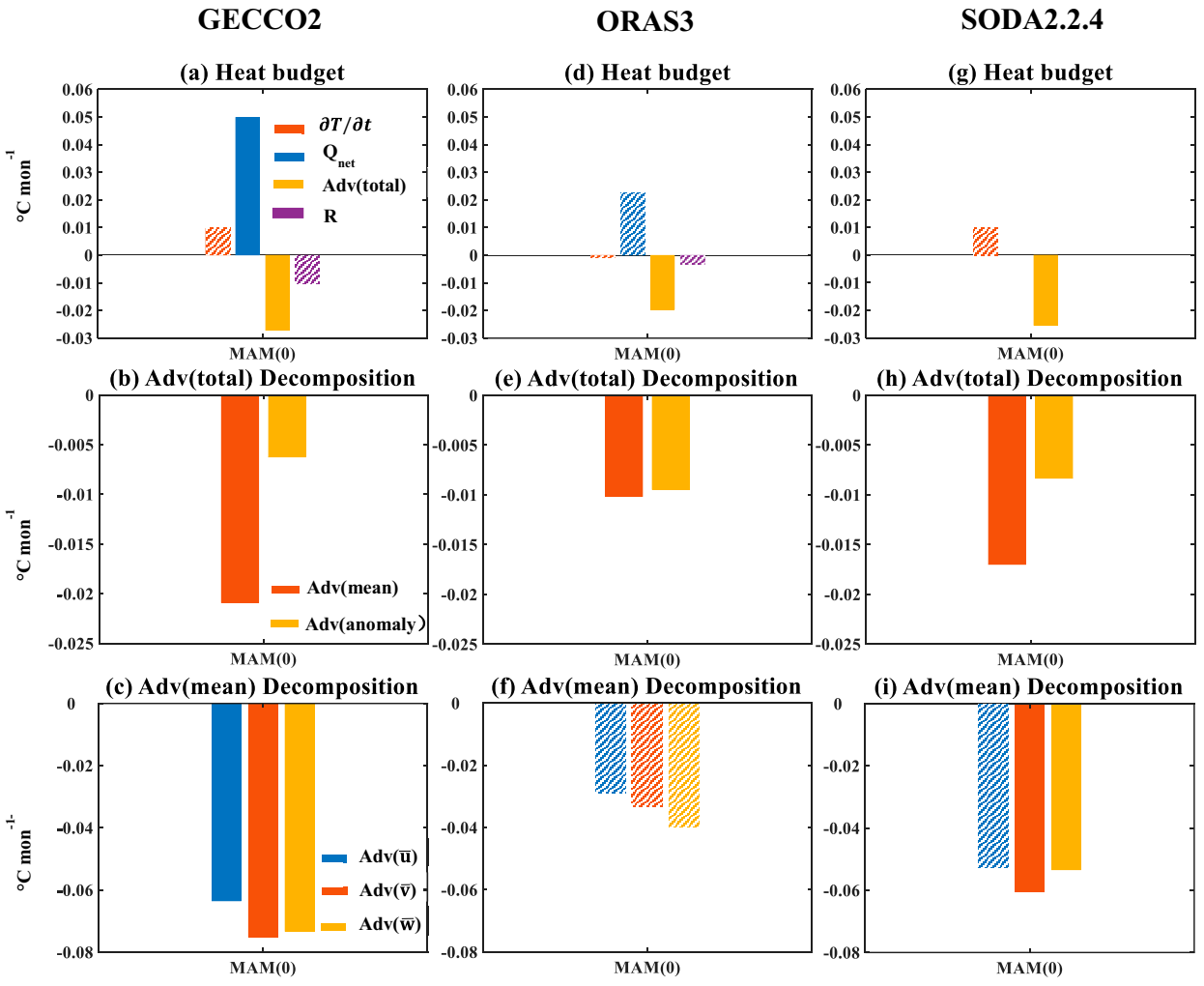

FIG. 10. As in Fig. 3, but for regressions of SPMM-associated oceanic heat advection terms in MAM(0) in the black boxes of the second row of Fig. 9.

(Fig. 8b) and propagate southwestward by the WES feedback from spring to summer (Figs. 8b,c). The feature of the equatorward propagation can be clearly seen from the zonal mean of the MLT anomalies in the region enclosed by the black lines (Figs. 8a–d). Specifically, in boreal winter, the anomalies slightly peak at ~23°N (blue line in Fig. 8m). In the following season, the anomalies become strongest and shift southward to ~19°N (red line in Fig. 8m). Then, they continue moving southward to 15°N in summer (yellow line in Fig. 8m) and are essentially stable in fall (purple line in Fig. 8m). In the DOM, the NPMM-related MLT anomalies can still propagate westward, similar to those in the SOM, but move northward instead of southward from boreal winter to summer (cf. Figs. 8a–h). This northward displacement can also be seen from the zonal mean of the MLT anomalies (Fig. 8n). Specifically, in boreal winter, the anomalies slightly peak at ~13°N; in spring, they exhibit a strong peak at ~17°N; and in summer, they move northward to ~19°N. The northward shifts of the zonal-mean maximum MLT anomaly or the center of the NPMM (denoted by the green markers in Figs. 8e–h) in boreal spring and summer are only attributed to the oceanic damping effects in the DOM (Figs. 7i,j). The feature of the northward movement can also be found in all the three reanalysis datasets. In the GECCO2, the zonal mean of the NPMM MLT anomalies slightly moves northward from ~21°N in D(−1)JF(0) to ~22°N in JJA(0) (Fig. 8o); in the ORAS3 and SODA2.2.4, the northward movement is even more noticeable [from ~20°N in D(−1)JF(0) to ~25°N in JJA(0); Fig. S4]. The consistency of the northward displacement between the model simulations and reanalysis datasets demonstrates the robustness of this finding.

4. Role of ocean advections during the evolution of the SPMM

a. *Diagnoses from the observational and reanalysis datasets*

In this section, we explore the role of ocean advections during the evolution of the SPMM. Figure 9 and Figs. S5 and S6

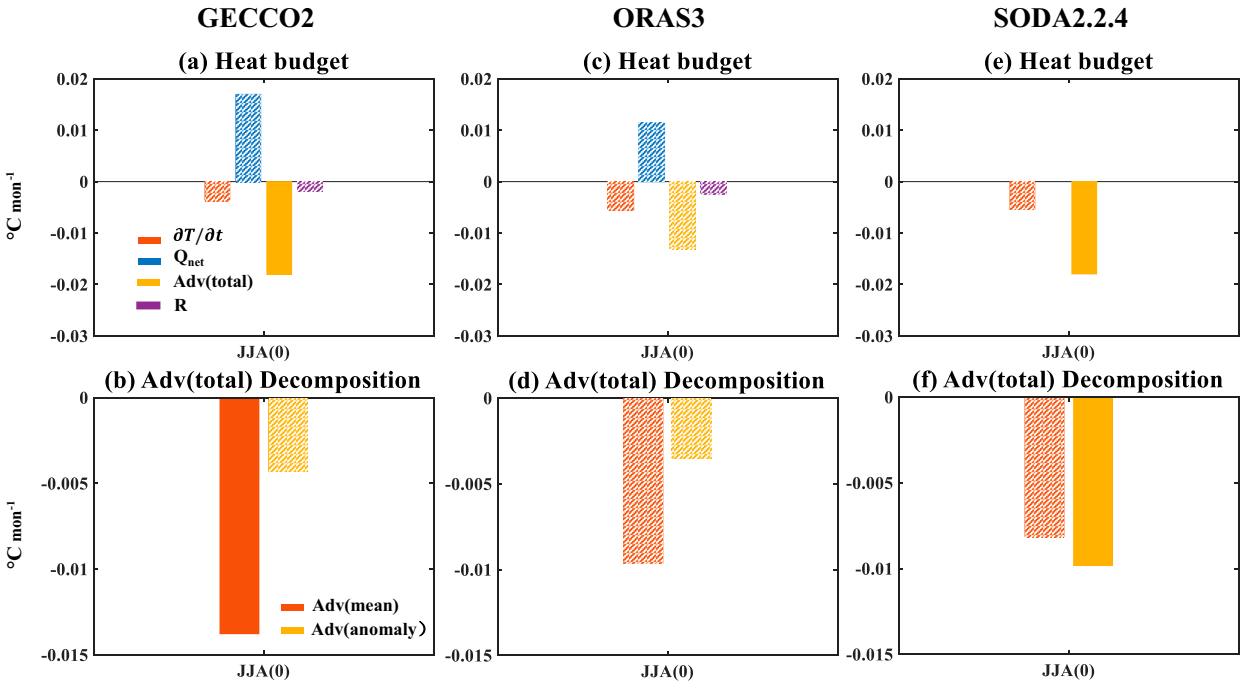

FIG. 11. As in Fig. 10, but for regressions of SPMM-associated oceanic heat advection terms in JJA(0) in the black boxes of the third row of Fig. 9.

show regressions of the tendency of MLT anomalies, net surface heat flux (no plots for the SODA2.2.4 are shown in Fig. S6), and total oceanic heat advection anomalies, as well as MLT anomalies south of 10°N against the SPMM index from D(−1)JF(0) to SON(0) in the GECCO2, ORAS3, and SODA2.2.4, respectively. The results show that in MAM(0), ocean advections play a role in damping MLT anomalies mostly in the center of the SPMM (Fig. 9j and Fig. S5j; weakest in the SODA2.2.4, as shown in Fig. S6f), compensating 54% (87% in the ORAS3) of the intensification effect by net heat flux anomalies, calculated by the absolute value of the yellow bar in Fig. 10a (Fig. 10d) divided by the blue bar in Fig. 10a (Fig. 10d). The strong compensating effect in MAM(0) may lead to the insignificant tendency of MLT anomalies (Fig. 9b, Figs. S5b and S6b). To further explore the damping, we regress anomalous heat advections by the mean and anomalous ocean current averaged over that region against the SPMM index. The results indicate that the damping effect in MAM(0) are primarily attributed to the anomalous heat advection by the mean ocean current (second row of Fig. 10). Further decompositions show that it is contributed by all 3D mean ocean currents, although the contribution is less significant in the ORAS3 (last row of Fig. 10).

The damping effect by 3D mean ocean currents sustains to JJA(0) in the GECCO2 (Fig. 9k) but is not significant averaged over the region in the ORAS3 (yellow bar in Fig. 11c). It is still weakest in the SODA2.2.4 (Fig. S6g). The damping effect in the GECCO2 compensates 106% of the intensification effect by net heat flux anomalies, calculated by absolute value of the yellow bar in Fig. 11a divided by the blue bar in Fig. 11a. The heat budget analysis indicates that the damping effect is significantly contributed from anomalous heat advection by the mean ocean current in the GECCO2 (Fig. 11b), opposed to the significant contribution from the anomalous ocean current in the SODA2.2.4 (Fig. 11f). Therefore, the damping effect by which anomalous heat advection term is quite uncertain across the three reanalysis datasets.

In addition to the damping effect, there exists an intensification effect southwest of the equatorial central Pacific in JJA(0) (purple boxes in Fig. 9k, Figs. S5k and S6g). Meanwhile, ENSO events begin to develop from the equatorial central Pacific toward eastern Pacific (contours in Fig. 9k, Figs. S5k and S6g). Given the close location between the intensification effect and ENSO development, whether the effect of ocean advections is related to the SPMM or the ENSO development is unclear. To investigate the problem, we regress total oceanic heat advection and SST anomalies against a residual SPMM index, which removes the following ENSO influence by regressing out ND(0)J(1) CTI from the SPMM index. The result shows that, in the absence of the following ENSO events, the intensification effect of ocean advections decreases but is still statistically significant (Figs. 12a,c,e, Figs. S7a,c,e and S8a,c,e). Furthermore, the heat budget analysis indicates that the intensification effect is dominated by anomalous heat advection by the mean ocean current (second row of Fig. 13). Further decomposition of the intensification effect of the mean ocean current exhibits diversity: in the GECCO2, the effect is dominated by the mean zonal current, while in the ORAS3 and SODA2.2.4, it is dominated by the mean meridional current (last row of Fig. 13).

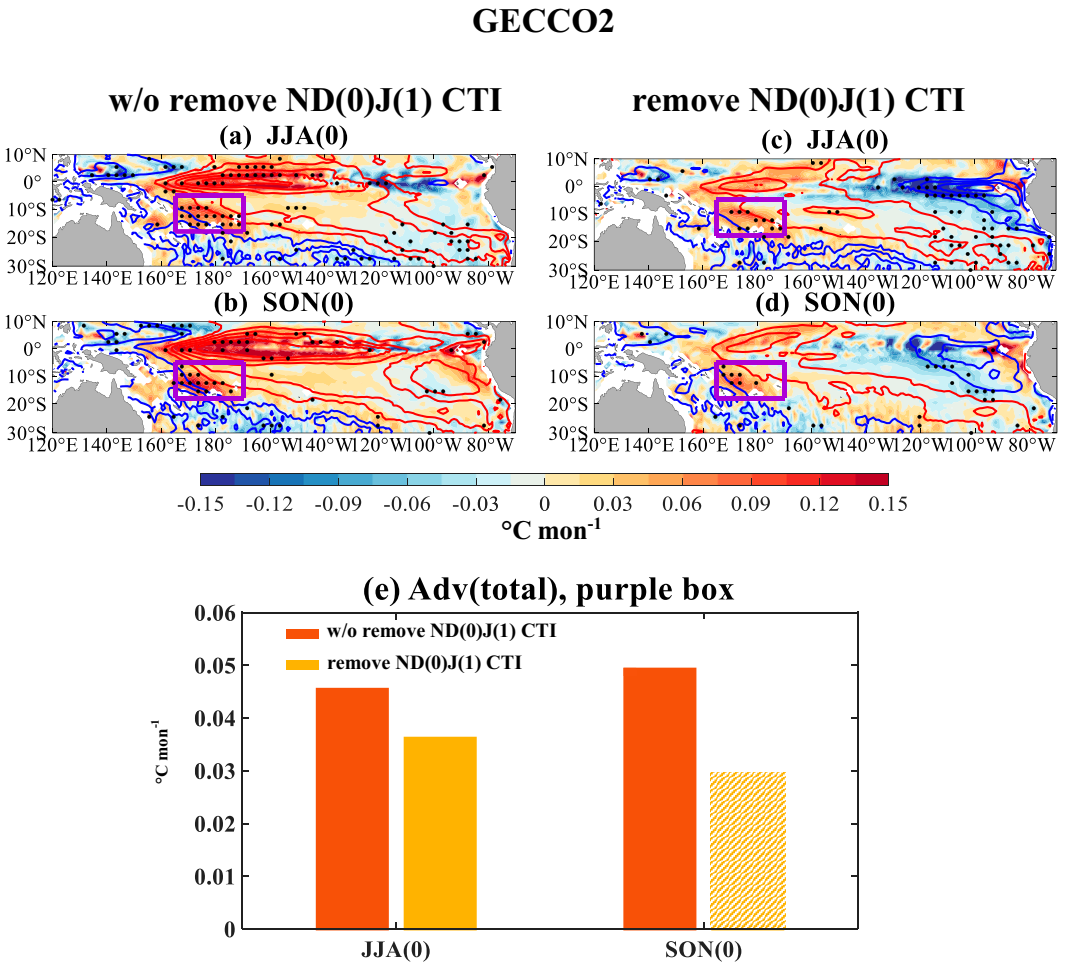

FIG. 12. (a),(b) Same plots as Figs. 9k and 9l. (c),(d) As in Figs. 9k and 9l, but for the regressions against a residual SPMM index, obtained by linearly removing ND(0)J(1) CTI from the SPMM index. Purple boxes are as in Fig. 9. (e) Regressed total oceanic heat advection anomalies averaged over the purple boxes.

In the following SON(0), the intensification effect still exists (Fig. 9l, Figs. S5l and S6h). To examine whether the effect is related to the SPMM or the following ENSO events, we also regress total oceanic heat advection and MLT anomalies against the residual SPMM index. The result shows that without the following ENSO events, the intensification effect weakens (Figs. 12b,d, Figs. S7b,d and S8b,d). Although the effect is still statistically significant in some regions southwest of the equatorial central Pacific (dots in the purple box in Fig. 12d, Figs. S7d and S8d), it becomes statistically insignificant when spatially averaged over the purple box (Fig. 12e, Figs. S7e and S8e). This insignificance suggests that the intensification effect is, to some extent, associated with the following ENSO.

b. Model simulations

In the last section, we diagnosed the roles of ocean advections in the SPMM evolution: damping effects in the center of the SPMM during boreal spring and summer and intensification effect in the southwest Pacific. In this section, we intend to reveal these effects on the SPMM evolution based on the model simulations.

First, we assess the simulation skill of the SPMM in the DOM (Fig. S9). It is found that some biases exist. First, the spatial pattern of the SPMM shifts northwestward (Fig. S9a) compared to the observations (Fig. 1f); second, the seasonality of SPMM-related SST and 10-m wind variabilities markedly differs from the observations (cf. Fig. 1h and Fig. S9c); and third, the greatest distinction is that the SPMM will not evolve into ENSO events (Fig. S9e and Fig. 14). Next, we evaluate the skill of the evolution of the SPMM-associated MLT and heat flux terms anomalies in the DOM (Fig. 14). The result shows that the SPMM-associated MLT anomalies have already spread northwestward in D(−1)JF(0) and gradually shrink toward the west coast of South America in JJA(0). The characteristic of this evolution contrasts to that in the observations, in which the SPMM-associated MLT anomalies develop from the west coast of South America in D(−1)JF(0) and propagate northwestward by JJA(0) (Fig. 9).

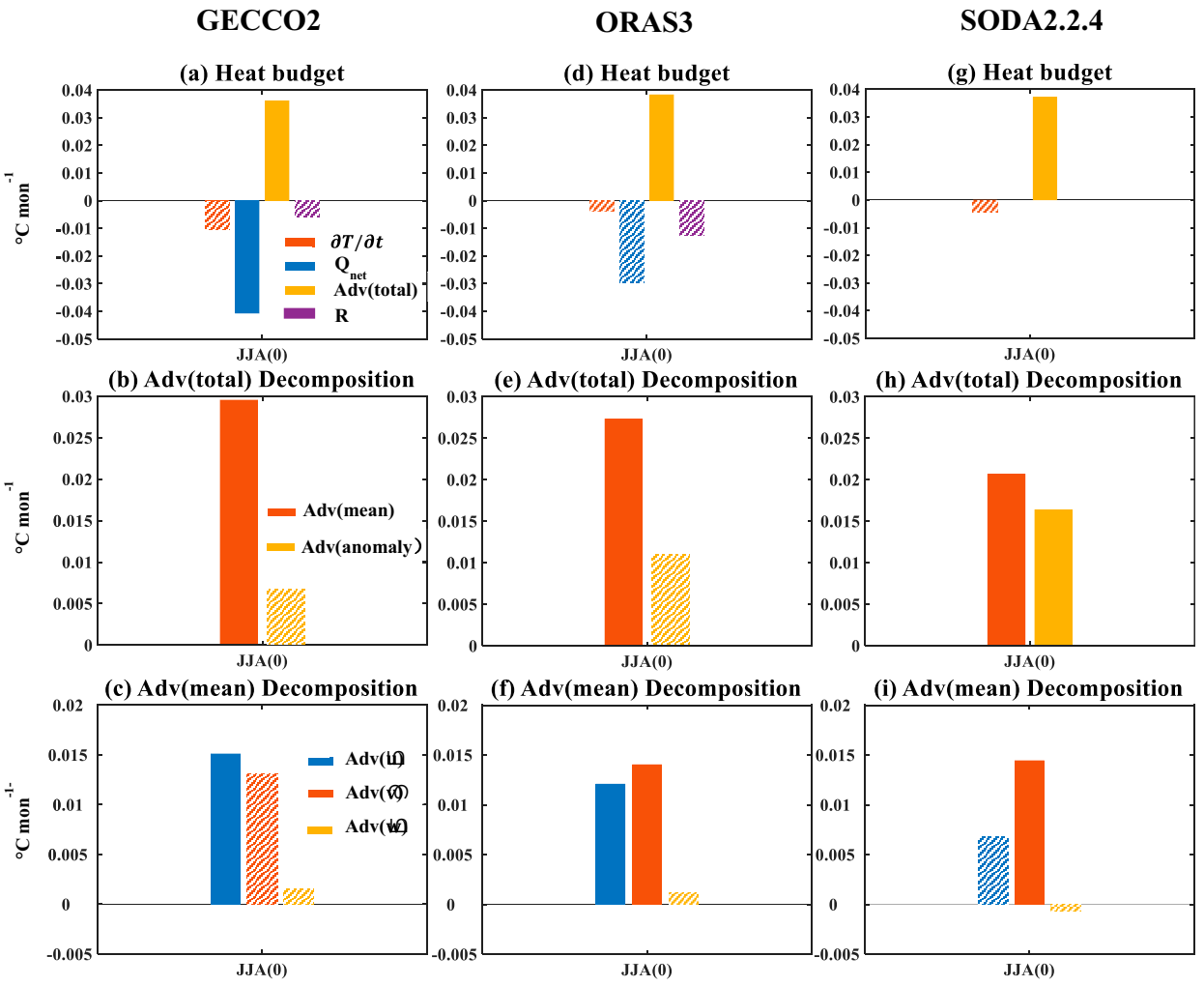

FIG. 13. As in Fig. 11, but for regressions of SPMM-associated oceanic heat advection terms against the residual SPMM index in JJA(0) in the purple boxes of Fig. 12.

Although the DOM simulates the roles of ocean advections in damping the center of the SPMM in boreal spring and summer (Figs. 14j,k) and in intensifying the SPMM-associated MLT anomalies in the southwest Pacific (Fig. 14k), the failure of the simulation of the SPMM evolution in the DOM leads to inconvincible explanation on the effects of ocean advections if comparing the DOM to SOM. In the future, we will systematically assess the simulation skill of the SPMM based on the DOMs from phase 6 of the Coupled Model Intercomparison Project (CMIP6) and compare their simulations to the corresponding SOM configuration.

5. Summary and discussion

We have demonstrated the role of ocean advections played during the evolutions of the NPMM and SPMM. First, we diagnosed their role by decomposing the anomalous oceanic heat advective terms in a mixed layer heat budget equation based on three ocean reanalysis products. Then, we revealed the effect of their role on the PMMs' evolution by comparing the simulation between the DOM and SOM.

Our analyses showed that, during the NPMM evolution, ocean advections play a damping role in the south of the NPMM center (Fig. 15a). They are primarily attributed to the anomalous meridional Ekman heat advections by anomalous, NPMM-related zonal wind stress from boreal winter to spring and by mean easterly trade winds during spring. The resulting damping effect shifts the NPMM northward from boreal winter to the following summer, instead of equatorward by the WES feedback, as suggested by previous studies (Chiang and Vimont 2004; Vimont et al. 2009; Wu et al. 2010; Ma et al. 2017; Min et al. 2017; Amaya 2019; Amaya et al. 2019; Yang et al. 2022). This finding is confirmed by the comparison between the DOM and SOM, as well as all the three ocean reanalysis products. It is also noted that the damping effect would not affect the NPMM westward propagation through the WES feedback, steered by the climatological easterly trade winds.

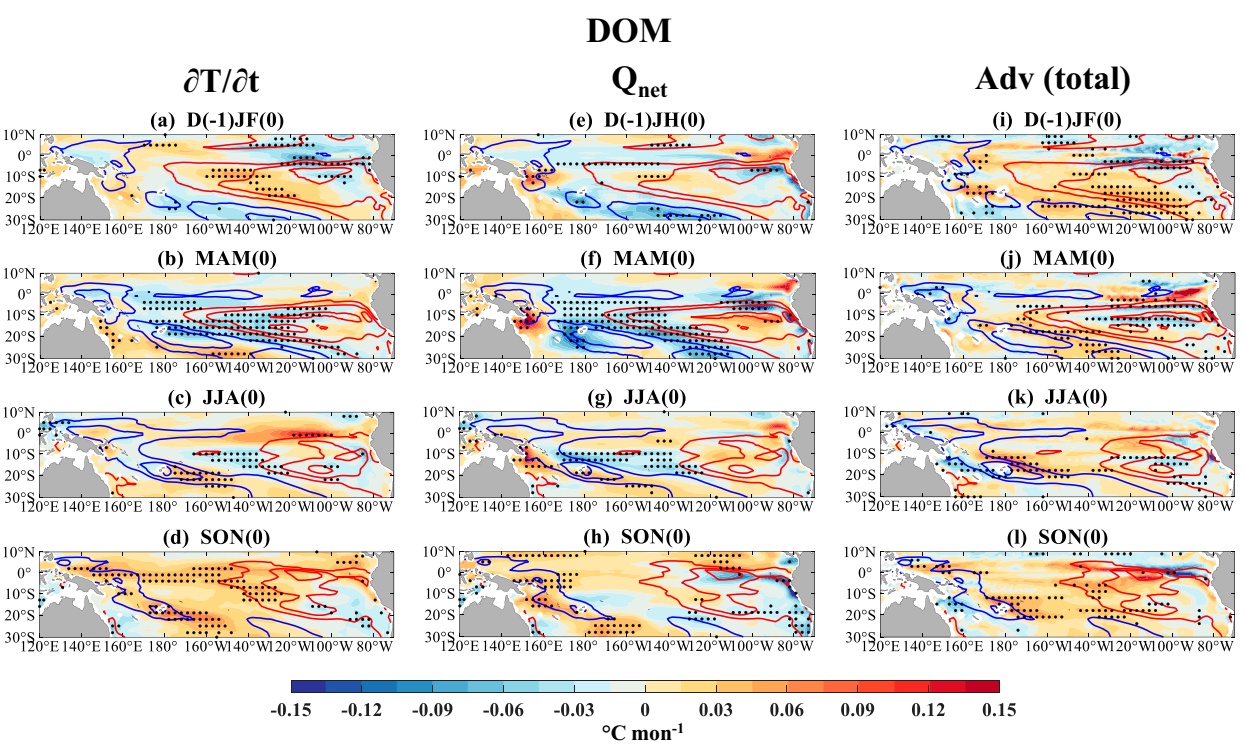

FIG. 14. As in Fig. 9, but for the SPMM evolution in the DOM.

During the SPMM evolution, ocean advections also play a damping role, but in the SPMM center, resulting in the SPMM weakened locally (Fig. 15b). Specifically, the ocean advective damping effect in boreal spring is mainly contributed by the mean ocean current, while in the ensuing summer, the contribution is unclear because of the large diversity across the three reanalysis datasets. In addition to the damping effect, an intensification effect by the mean ocean current emerges in the southwest Pacific in boreal summer. However, its effect on the SPMM evolution is unknown due to the strong simulation bias of the SPMM evolution in the DOM. Therefore, we encourage exploration of this issue based on other state-of-the-art climate models, such as the CMIP6, in future studies.

The finding of the northward shift of the NPMM induced by the ocean advective damping inspires us to pay more attention to diagnosing the heat budget terms in the vicinity of the MLT or SST maxima, rather than in their local region, which was typically used in previous studies, such as investigating the controlling factor of subtropical North Pacific SST anomalies mentioned in the Introduction (Larson et al. 2018b; Middlemas et al. 2019; Small et al. 2020; Takahashi et al. 2021). This approach may help explain the dynamics of spatiotemporally evolved SST variability in future research.

Acknowledgments. We sincerely appreciate the editor Dr. Agus Santoso and three anonymous reviewers who provide constructive comments to substantially improve the manuscript. Y. Z. and X. L. were supported by the National Natural Science Foundation of China (Grants 41925025 and 92058203). Y. Z. was supported by the Fundamental Research Funds for the Central Universities (Grant 202213050), the project funded by China Postdoctoral Science Foundation (Grant 2021M703034) and Laoshan Laboratory (Grant LSKJ202202602). S. M. L. was supported by the National Science Foundation (Grant AGS-1951713). Y. K. was supported by the Japan Society for the Promotion of Science (Grants JP19H05703 and JP22H01302) and the Japanese Ministry of Education, Culture, Sports, Science and Technology (Grants JPMXD0717935457 and JPMXD0722680395). J.-C. Y. was supported by the National Natural Science Foundation of China (Grants 42105019 and 92058203).

Data availability statement. The HadISSTv1.1 data are available at https://www.metoffice.gov.uk/hadobs/hadisst/data/download.html. The 20CRv3 data are available at https://psl.noaa.gov/data/gridded/data.20thC_ReanV3.monolevel.html#caveat. The GECCO2 data are available at https://icdc.cen.uni-hamburg.de/thredds/catalog/ftpthredds/EASYInit/GECCO2/regular_1x1_grid/catalog.html. The ORAS3 data are available at http://apdrc.soest.hawaii.edu/erddap/search/index.html?page=1&itemsPerPage=1000&searchFor=ORA-S3. The SODA2.2.4 data are available at http://apdrc.soest.hawaii.edu/erddap/search/index.html?page=1&itemsPerPage=1000&searchFor=SODA. The SOM outputs are available at https://nomads.gfdl.noaa.gov/dods-data/gfdl_sm2_1/MLM2.1U_Control-1990_D1/pp/. The DOM outputs are available at https://doi.org/10.5281/zenodo.7297143.

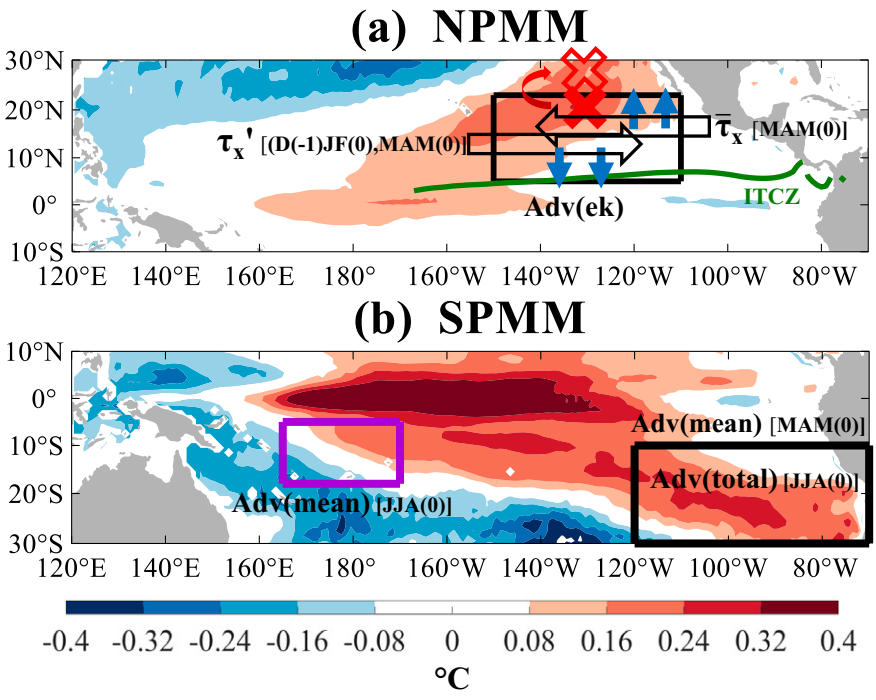

FIG. 15. Schematics of the roles of oceanic advections during the evolution of the (a) NPMM and (b) SPMM. Shading shows the NPMM-related MLT anomalies averaged over D(−1)JF(0) and MAM(0) and SPMM-related MLT anomalies in JJA(0). Black boxes delineate the region in which ocean advections play a damping role. The purple box is the region in which ocean advections play an intensification role; Blue arrows indicate the damping effect by anomalous Ekman heat advection. The green line shows the location of the climatological ITCZ averaged over DJF and MAM. Red markers indicate the NPMM center and its shift to the north. Abbreviations are as follows: Adv(ek), anomalous heat advection by the Ekman current; Adv(total), anomalous heat advection by the mean and anomalous 3D ocean current; Adv(mean), anomalous heat advection by the mean 3D ocean current.

REFERENCES

Alexander, M. A., D. J. Vimont, P. Chang, and J. D. Scott, 2010: The impact of extratropical atmospheric variability on ENSO: Testing the seasonal footprinting mechanism using coupled model experiments. *J. Climate*, **23**, 2885–2901, https://doi.org/10.1175/2010JCLI3205.1.

Amaya, D. J., 2019: The Pacific meridional mode and ENSO: A review. *Curr. Climate Change Rep.*, **5**, 296–307, https://doi.org/10.1007/s40641-019-00142-x.

——, Y. Kosaka, W. Zhou, Y. Zhang, S.-P. Xie, and A. J. Miller, 2019: The North Pacific pacemaker effect on historical ENSO and its mechanisms. *J. Climate*, **32**, 7643–7661, https://doi.org/10.1175/JCLI-D-19-0040.1.

Anderson, B. T., 2007: Intraseasonal atmospheric variability in the extratropics and its relation to the onset of tropical Pacific sea surface temperature anomalies. *J. Climate*, **20**, 926–936, https://doi.org/10.1175/JCLI4036.1.

——, and R. C. Perez, 2015: ENSO and non-ENSO induced charging and discharging of the equatorial Pacific. *Climate Dyn.*, **45**, 2309–2327, https://doi.org/10.1007/s00382-015-2472-x.

——, ——, and A. Karspeck, 2013: Triggering of El Niño onset through trade wind–induced charging of the equatorial Pacific. *Geophys. Res. Lett.*, **40**, 1212–1216, https://doi.org/10.1002/grl.50200.

Balmaseda, M. A., A. Vidard, and D. L. T. Anderson, 2008: The ECMWF ocean analysis system: ORA-S3. *Mon. Wea. Rev.*, **136**, 3018–3034, https://doi.org/10.1175/2008MWR2433.1.

Carton, J. A., and B. S. Giese, 2008: A reanalysis of ocean climate using Simple Ocean Data Assimilation (SODA). *Mon. Wea. Rev.*, **136**, 2999–3017, https://doi.org/10.1175/2007MWR1978.1.

Chakravorty, S., R. C. Perez, B. T. Anderson, S. M. Larson, B. S. Giese, and V. Pivotti, 2021: Ocean dynamics are key to extratropical forcing of El Niño. *J. Climate*, **34**, 8739–8753, https://doi.org/10.1175/JCLI-D-20-0933.1.

Chang, P., L. Zhang, R. Saravanan, D. J. Vimont, J. C. H. Chiang, L. Ji, H. Seidel, and M. K. Tippett, 2007: Pacific meridional mode and El Niño–Southern Oscillation. *Geophys. Res. Lett.*, **34**, L16608, https://doi.org/10.1029/2007GL030302.

Chiang, J. C. H., and D. J. Vimont, 2004: Analogous Pacific and Atlantic meridional modes of tropical atmosphere–ocean variability. *J. Climate*, **17**, 4143–4158, https://doi.org/10.1175/JCLI4953.1.

Delworth, T. L., and Coauthors, 2006: GFDL's CM2 global coupled climate models. Part I: Formulation and simulation characteristics. *J. Climate*, **19**, 643–674, https://doi.org/10.1175/JCLI3629.1.

Deser, C., and J. M. Wallace, 1990: Large-scale atmospheric circulation features of warm and cold episodes in the tropical

Pacific. *J. Climate*, **3**, 1254–1281, https://doi.org/10.1175/1520-0442(1990)003<1254:LSACFO>2.0.CO;2.

Kim, J. W., and J.-Y. Yu, 2021: Evolution of subtropical Pacific-onset El Niño: How its onset location controls its decay evolution. *Geophys. Res. Lett.*, **48**, e2020GL091345, https://doi.org/10.1029/2020GL091345.

Kim, S.-B., T. Lee, and I. Fukumori, 2007: Mechanisms controlling the interannual variation of mixed layer temperature averaged over the Niño-3 region. *J. Climate*, **20**, 3822–3843, https://doi.org/10.1175/JCLI4206.1.

Köhl, A., 2015: Evaluation of the GECCO2 ocean synthesis: Transports of volume, heat and freshwater in the Atlantic. *Quart. J. Roy. Meteor. Soc.*, **141**, 166–181, https://doi.org/10.1002/qj.2347.

Larson, S. M., and B. P. Kirtman, 2013: The Pacific meridional mode as a trigger for ENSO in a high-resolution coupled model. *Geophys. Res. Lett.*, **40**, 3189–3194, https://doi.org/10.1002/grl.50571.

——, and ——, 2014: The Pacific meridional mode as an ENSO precursor and predictor in the North American multimodel ensemble. *J. Climate*, **27**, 7018–7032, https://doi.org/10.1175/JCLI-D-14-00055.1.

——, K. V. Pegion, and B. P. Kirtman, 2018a: The South Pacific meridional mode as a thermally driven source of ENSO amplitude modulation and uncertainty. *J. Climate*, **31**, 5127–5145, https://doi.org/10.1175/JCLI-D-17-0722.1.

——, D. J. Vimont, A. Clement, and B. P. Kirtman, 2018b: How momentum coupling affects SST variance and large-scale Pacific climate variability in CESM. *J. Climate*, **31**, 2927–2944, https://doi.org/10.1175/JCLI-D-17-0645.1.

Ma, J., S.-P. Xie, and H. Xu, 2017: Contributions of the North Pacific meridional mode to ensemble spread of ENSO prediction. *J. Climate*, **30**, 9167–9181, https://doi.org/10.1175/JCLI-D-17-0182.1.

Middlemas, E., A. Clement, and B. Medeiros, 2019: Contributions of atmospheric and oceanic feedbacks to subtropical northeastern sea surface temperature variability. *Climate Dyn.*, **53**, 6877–6890, https://doi.org/10.1007/s00382-019-04964-1.

Min, Q., J. Su, and R. Zhang, 2017: Impact of the South and North Pacific meridional modes on the El Niño–Southern Oscillation: Observational analysis and comparison. *J. Climate*, **30**, 1705–1720, https://doi.org/10.1175/JCLI-D-16-0063.1.

Rayner, N. A., D. E. Parker, E. B. Horton, C. K. Folland, L. V. Alexander, D. P. Rowell, E. C. Kent, and A. Kaplan, 2003: Global analyses of sea surface temperature, sea ice, and night marine air temperature since the late nineteenth century. *J. Geophys. Res.*, **108**, 4407, https://doi.org/10.1029/2002JD002670.

Rogers, J. C., 1981: The North Pacific Oscillation. *J. Climatol.*, **1**, 39–57, https://doi.org/10.1002/joc.3370010106.

Slivinski, L. C., and Coauthors, 2019: Towards a more reliable historical reanalysis: Improvements for version 3 of the Twentieth Century Reanalysis system. *Quart. J. Roy. Meteor. Soc.*, **145**, 2876–2908, https://doi.org/10.1002/qj.3598.

Small, R. J., F. O. Bryan, S. P. Bishop, S. Larson, and R. A. Tomas, 2020: What drives upper-ocean temperature variability in coupled climate models and observations? *J. Climate*, **33**, 577–596, https://doi.org/10.1175/JCLI-D-19-0295.1.

Stevenson, J. W., and P. P. Niiler, 1983: Upper ocean heat budget during the Hawaii-to-Tahiti shuttle experiment. *J. Phys. Oceanogr.*, **13**, 1894–1907, https://doi.org/10.1175/1520-0485(1983)013<1894:UOHBDT>2.0.CO;2.

Stuecker, M. F., 2018: Revisiting the Pacific meridional mode. *Sci. Rep.*, **8**, 3216, https://doi.org/10.1038/s41598-018-21537-0.

Takahashi, N., K. J. Richards, N. Schneider, H. Annamalai, W. C. Hsu, and M. Nonaka, 2021: Formation mechanism of warm SST anomalies in 2010s around Hawaii. *J. Geophys. Res. Oceans*, **126**, e2021JC017763, https://doi.org/10.1029/2021JC017763.

Vimont, D. J., M. Alexander, and A. Fontaine, 2009: Midlatitude excitation of tropical variability in the Pacific: The role of thermodynamic coupling and seasonality. *J. Climate*, **22**, 518–534, https://doi.org/10.1175/2008JCLI2220.1.

Walker, G. T., and E. W. Bliss, 1932: World weather V. *Mem. Roy. Meteor. Soc.*, **4**, 53–84.

Wu, S., L. Wu, Q. Liu, and S.-P. Xie, 2010: Development processes of the tropical Pacific meridional mode. *Adv. Atmos. Sci.*, **27**, 95–99, https://doi.org/10.1007/s00376-009-8067-x.

Xie, S.-P., and S. G. H. Philander, 1994: A coupled ocean-atmosphere model of relevance to the ITCZ in the eastern Pacific. *Tellus*, **46A**, 340–350, https://doi.org/10.3402/tellusa.v46i4.15484.

Yang, J.-C., Y. Zhang, X. Lin, and P. Chang, 2021: Optimal growth of IPV lags AMV modulations by up to a decade. *Geophys. Res. Lett.*, **48**, e2021GL096654, https://doi.org/10.1029/2021GL096654.

Yang, L., S.-P. Xie, S. S. P. Shen, J.-W. Liu, and Y.-T. Hwang, 2022: Low cloud-SST feedback over the subtropical northeast Pacific and the remote effect on ENSO variability. *J. Climate*, **36**, 441–452, https://doi.org/10.1175/JCLI-D-21-0902.1.

Yeh, S.-W., H.-S. Jo, S.-H. Hyun, W. Cai, and Y.-G. Ham, 2021: Role of the eastern subtropical North Pacific Ocean on the El Niño's transition processes. *Climate Dyn.*, **56**, 1285–1301, https://doi.org/10.1007/s00382-020-05530-w.

You, Y., and J. C. Furtado, 2017: The role of South Pacific atmospheric variability in the development of different types of ENSO. *Geophys. Res. Lett.*, **44**, 7438–7446, https://doi.org/10.1002/2017GL073475.

——, and ——, 2018: The South Pacific meridional mode and its role in tropical Pacific climate variability. *J. Climate*, **31**, 10 141–10 163, https://doi.org/10.1175/JCLI-D-17-0860.1.

Zhang, H., A. Clement, and P. Di Nezio, 2014: The South Pacific meridional mode: A mechanism for ENSO-like variability. *J. Climate*, **27**, 769–783, https://doi.org/10.1175/JCLI-D-13-00082.1.

Zhang, Y., and Coauthors, 2021: Pacific meridional modes without equatorial Pacific influence. *J. Climate*, **34**, 5285–5301, https://doi.org/10.1175/JCLI-D-20-0573.1.

——, and Coauthors, 2022a: Role of ocean dynamics in equatorial Pacific decadal variability. *Climate Dyn.*, **59**, 2517–2529, https://doi.org/10.1007/s00382-022-06312-2.

——, S.-Y. Yu, D. J. Amaya, Y. Kosaka, M. F. Stuecker, J.-C. Yang, X. Lin, and L. Fan, 2022b: Atmospheric forcing of the Pacific meridional mode: Tropical Pacific-driven versus internal variability. *Geophys. Res. Lett.*, **49**, e2022GL098148, https://doi.org/10.1029/2022GL098148.